Inside Cover: Nanosecond Dynamics of Calmodulin and Ribosome-Bound Nascent Chains Studied by Time-Resolved Fluorescence Anisotropy (ChemBioChem 7/2014)

ARTICLE *in* CHEMBIOCHEM · MAY 2014

Impact Factor: 3.09 · DOI: 10.1002/cbic.201400014

DOI: 10.1002/cbic.201400014

Nanosecond Dynamics of Calmodulin and Ribosome-Bound Nascent Chains Studied by Time-Resolved Fluorescence Anisotropy

Paraskevas Lamprou,[a] Daryan Kempe,[b] Alexandros Katranidis,[a] Georg Büldt,[a, c] and Jörg Fitter*[a, b]

We report a time-resolved fluorescence anisotropy study of ribosome-bound nascent chains (RNCs) of calmodulin (CaM), a prototypical member of the EF-hand family of calcium-sensing proteins. As shown in numerous studies, in vitro protein refolding can differ substantially from biosynthetic protein folding, which takes place cotranslationally and depends on the rate of polypeptide chain elongation. A challenge in this respect is to characterize the adopted conformations of nascent chains before their release from the ribosome. CaM RNCs (full-length, half-length, and first EF-hand only) were synthesized in vitro. All constructs contained a tetracysteine motif site-specifically incorporated in the first N-terminal helix; this motif is known to react with FlAsH, a biarsenic fluorescein derivative. As the dye is rotationally locked to this helix, we characterized the structural properties and folding states of polypeptide chains tethered to ribosomes and compared these with released chains. Importantly, we observed decelerated tumbling motions of ribosome-tethered and partially folded nascent chains, compared to released chains. This indicates a pronounced interaction between nascent chains and the ribosome surface, and might reflect chaperone activity of the ribosome.

Introduction

In living cells, folding of proteins starts during their synthesis, while the nascent polypeptide chain is still tethered to the ribosome.[1–4] As the information required for proteins to adopt their native conformation is generally encoded in the amino acid sequence, the polypeptide chains also fold in vitro (in the absence of the cellular environment).[5] In most folding studies, the transition of a full-length polypeptide chain from an unfolded state to a folded state is monitored. It has been shown that significant differences in folding occur between de novo synthesized proteins at the ribosome and classical (re-)folding. In particular, for multidomain proteins, folding of de novo synthesized proteins proceeds from one domain to the next, whereas the situation is completely different for the refolding of full-length polypeptide chains.[6] As a consequence, folding rates and the characteristics of folding intermediates can differ.[7,8] Although cotranslational folding and an understanding how polypeptide chain elongation and folding are coupled are interesting topics, only a few studies have been performed.[1,2,7,9–13] This might be attributable to the fact that studying cotranslational folding is much more laborious than classical refolding studies. One of the main difficulties in cotranslational folding studies is experimental access to the structural properties of ribosome-bound nascent chains. Typically, ribosome-bound nascent chains (RNCs) are produced in cell-free expression systems, which provide rather low yields. Therefore fluorescence-based techniques are advantageous because they offer very high sensitivity, ideally suited for samples with low molar concentrations. One important prerequisite for this approach is to have RNCs that are labeled with fluorescent dyes. The most elegant way is to incorporate cotranslationally fluorescent non-natural amino acids in the nascent chain by use of the t-RNA suppressor technique.[9,11,14,15] Alternatively, labeling of RNCs can be carried out post-translationally. For this, one has to choose a chemical binding mechanism such that the dye exclusively targets the RNC (not the ribosome or other proteins in a cell-free expression system). Examples have used click chemistry[16] or biarsenical ligands that bind to tetracysteine motifs.[17] The advantage of biarsenical fluorescent dyes is that these are anchored more rigidly to the proteins by a tetracoordinate linkage. This enables more direct probing of the rotational dynamics of proteins (without the influence of random dye–probe motion). Fluorescence anisotropy measurements give direct experimental access to the rotational dynamics of whole proteins, as well as to the motions of helices or of domains.[17–19]

To assess the possibility of studying RNC conformations by time-resolved fluorescence anisotropy (TRA) we performed a study with the small two-domain protein calmodulin (CaM).

[a] Dr. P. Lamprou,[+] Dr. A. Katranidis, Prof. G. Büldt, Prof. J. Fitter
Institute of Complex Systems (ICS-5): Molecular Biophysics
Research Centre Jülich
Wilhelm-Johnen Strasse, 52425 Jülich (Germany)
E-mail: j.fitter@fz-juelich.de

[b] D. Kempe,[+] Prof. J. Fitter
I. Physikalisches Institut (IA), RWTH Aachen University
Sommerfeldstrasse 14, 52074 Aachen (Germany)

[c] Prof. G. Büldt
Laboratory of Advanced Studies of Membrane Proteins
Moscow Institute of Physics and Technology
9 Institutskiy per, 141700 Dolgoprudniy (Russia)

[+] These authors contributed equally to this work.

CaM is involved in signaling pathways related to calcium-dependent modulation of the functions of numerous target proteins, such as ion channels and kinases.[20,21] Calcium ions bind to four EF-hand structures (two in each globular domain). The biarsenical dye FlAsH binds to a tetracysteine motif that can be introduced into the N-terminal helix A of CaM.[17] Several anisotropy studies have been performed, mainly to investigate conformational changes upon calcium binding or segment motion.[18,19,22] We took advantage of this approach (FlAsH bound to a tetracysteine motif in helix A) to investigate the dynamic properties of CaM RNCs synthesized to different lengths. The data from TRA measurements were analyzed by multicomponent fits to extract rotational correlation times and parameters determining the geometry of the rotational motion. This information was used to gain insights into the structural and dynamic properties of the individual CaM constructs.

Results and Discussion

Production, characterization and labeling of CaM constructs

To obtain CaM with a rigidly attached dye we first mutated full-length CaM by incorporating a tetracysteine motif (E7C, E8C, A11C, E12C) in the N-terminal helix A (Figure 1). After

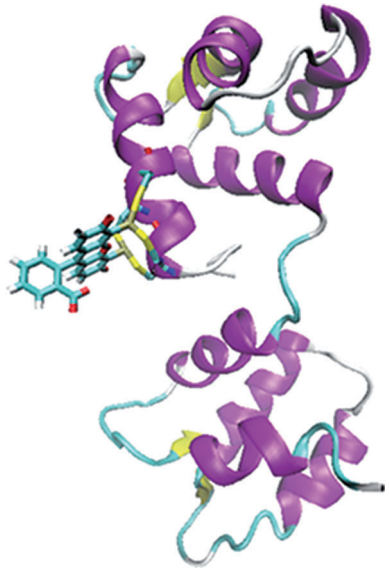

Figure 1. FlAsH bound to the tetra-Cys motif at the N-terminal helix A of calmodulin. The apo-protein (without calcium) is shown (PDB ID: 1DMO). Structure representations were produced in PyMOL (DeLano Scientific, San Carlos, CA).

overexpression in *Escherichia coli* and purification, we checked the product by using CD spectroscopy (Figure 3).

For our full-length mutant we observed that the secondary structure content was somewhat reduced (<10%) relative to wild-type CaM. This indicates that the mutated full-length CaM structure remains almost unchanged. The success of the subsequent labeling reactions was verified by observation of the characteristic red-shift of the FlAsH fluorescence emission spectrum; this only occurs upon linkage formation with the tetracysteine motif.[23] Furthermore, a significant increase in emission intensity was observed upon FlAsH binding. In order to obtain information about the emerging structure of a nascent chain during elongation, we started with a series of "snapshots" of this process, by looking at truncated CaM constructs: the first EF-hand (residues 1–40), half-length CaM (1–78), and full-length protein (1–149; Figure 2) To a certain extent, these

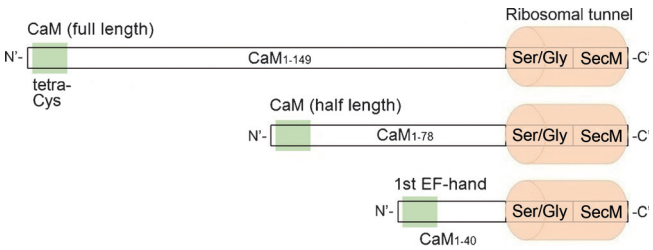

Figure 2. RNC complexes with CaM sequences of different lengths. For cell-free biosynthesis a linker sequence (26 aa; spanning the ribosomal tunnel) and a SecM-arrest sequence (17 aa; suppressing the release from the ribosome) are added.

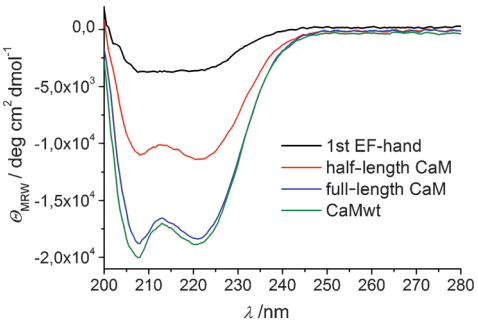

Figure 3. CD spectra of CaM constructs of different chain lengths, with wild-type CaM for reference. The fraction of α-helix content decreases with decreasing chain length.

structures correspond to structures at specific stages during cotranslational folding.

We first produced these CaM constructs by overexpression in *E. coli*. For this protein synthesis we used constructs without the linker and SecM-arrest sequence (Figure 2). The purified products were analyzed by CD spectroscopy in order to examine the degree of folding. The EF-hand construct included two α-helices, and the half-length CaM had four α-helices. With respect to the total chain length, the relative content of secondary-structure elements should be rather similar for all constructs.

However, our CD signal (mean residue ellipticity $[\Theta]_{MRW}$, which is normalized to the number of amino acids in the polypeptide chain) clearly shows decreasing relative secondary structure content with decreasing chain length (Figure 3). Compared to full-length CaM, the half-length CaM and the first EF-hand exhibited only ~50 and ~25% α-helix content, respectively. Evidently, the shorter constructs do not adopt a fully

folded state (see native full-length protein in Figure 1). A similar result was obtained in a NMR study on immunoglobulin domains.[10] This observation indicates that structure formation (here, of α-helices) requires not only the amino acids building blocks of the respective secondary structure element, but also amino acids downstream in the polypeptide sequence.

Fluorescence anisotropy decay of full-length FlAsH-CaM complexes

The purpose of measuring anisotropy decays is to obtain structural information about the polypeptide chain by monitoring the fluorescence properties of a single dye attached to the chain. As the dye in this study was rigidly bound to a tetracysteine motif in an N-terminal α-helix (residues 7–19) we measured rotational motion of this structural element by analyzing anisotropy decay. Furthermore, the fluorescence life-time of FlAsH (τ between 3 and 4 ns) determines the time window of rotational motions for which our method is sensitive. In this time regime, in addition to the overall rotation of the entire protein, movements of smaller protein segments (e.g., helix, domain) can contribute to anisotropy decay. To exemplify the general properties of the FlAsH–CaM complex, anisotropy decays were measured with in vivo synthesized full-length apo-CaM and calcium activated CaM (Figure 4C and D). In addition, as a further example of a rigidly bound fluorophore, we tested green fluorescence protein (wt-GFP purchased from Life Technologies), where the chromophore is crosslinked in the center of a β-barrel structure[24] (Aequorea Victoria GFP, Sino Biological Inc., Beijing, China, catalogue number: 13105-S07E; Figure 4A). For a fourth example, we analyzed a conventionally attached dye (Alexa 488 malemide; Figure 4B) bound to a cysteine residue in the structure of phosphoglycerate kinase (PGK).[25] Details about this construct are given in ref. [25].

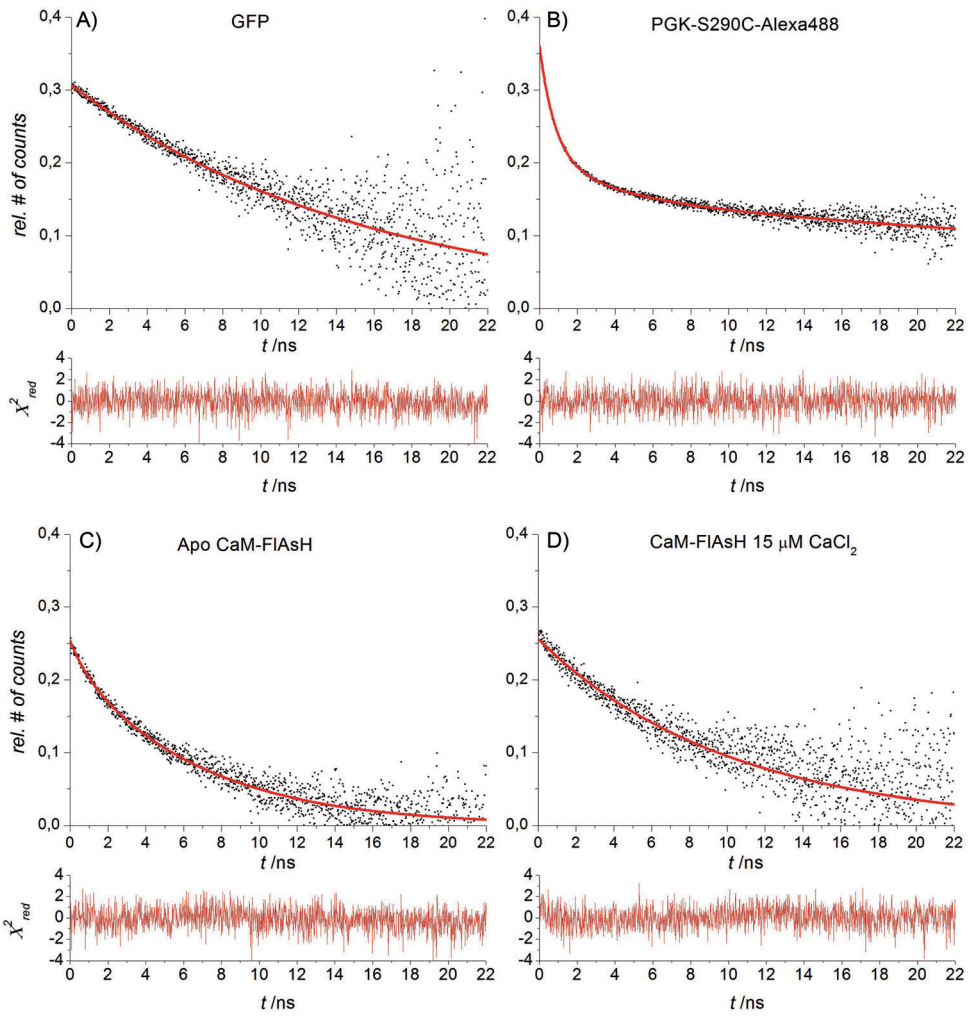

Figure 4. Time-resolved anisotropy decays for A) GFP, B) Alexa 488-labeled PGK, C) FlAsH-labeled apo-CaM, and D) FlAsH-labeled CaM-Ca^{2+}.

The obtained anisotropy decays (see the Experimental Section) were fitted with models described in detail by Schröder et al.[26] Here we consider in the most general case three decay components, namely a fast sub-nanosecond dynamics of the attached dye, a slower motion of protein segments (loop, helix, domain), and the even slower overall tumbling of the whole molecule [Eq. (3)]. The results of the fits based on this approach are shown in Table 1. In the case of very good statistics, we were able to resolve three components for Alexa 488-labeled PGK. In addition to fast dye motion (θ_2, A_2) we obtained for this medium-sized two-domain protein a segment motion with a correlation time in the order of a few nanoseconds (θ_1, A_1), which is most probably related to interdomain movements. Finally, we observed a rather slow correlation time (θ_M) for the overall tumbling of the protein; this is related to the molecule size if a spherical particle is assumed,[27]

$$\theta_M = \frac{\eta V}{RT} = \frac{\eta M_w (h + \upsilon)}{RT} \quad (1)$$

where η is buffer viscosity, T is the absolute temperature, and R is the gas constant. The effective volume of the tumbling unit (V) is determined from the molecular mass (M_w) of the protein; υ is the inverse specific density of a folded protein (~0.73–0.8 mL g^{-1}); h accounts for the hydration of the protein (0.23 g H_2O per g protein).[28]

Table 1. Fitting parameter obtained from data of labeled proteins[a] shown in Figure 4.[b]

Sample	r_0	θ_1 [ns]	A_1	θ_2 [ns]	A_2	θ_M [ns]
GFP	0.307[c] [0.306–0.308]	–	–	–	–	15.53 [15.39–15.68]
PGK	0.356 [0.355–0.358]	4.4 [3.3–6.2]	0.72 [0.66–0.75]	0.87 [0.83–0.9]	0.58 [0.56–0.61]	72.3 [58.5–108.4]
CaM [apo]	0.253 [0.251–0.256]	1.01 [0.76–1.34]	0.89 [0.875–0.91]	–	–	6.597 [6.44–6.77]
CaM [Ca^{2+}]	0.256 [0.255–0.257]	–	–	–	–	10.10 [9.96–10.25]

[a] Full-length CaM (17.8 kDa) labeled with FlAsH, GFP (26.9 kDa; fluorescence lifetime $\tau \sim 3$ ns), and PGK labeled with Alexa 488 (45.3 kDa; $\tau \sim 3$ ns). [b] The fitting models are detailed in the Experimental Section. [c] The confidence interval is given in brackets, see the Experimental Section.

For PGK the obtained correlation time θ_M was somewhat slower than expected from Equation (1) ($\theta_M \approx 50$ ns). Besides effects arising from deviation from a spherical shape, the fluorescence lifetime of the dye (see legend of Table 1) is too small to reproduce slow tumbling rates of larger molecules with a high precision (see also large range of θ_M values for the confidence interval). Due to the rigidly bound chromophore in GFP the measured anisotropy decay could be fitted with a single decay component; this is rather slow and describes the overall protein rotation. The obtained value is in agreement with the theoretically expected one.

For apo-CaM-FlAsH we observe a biphasic anisotropy decay, but the fast decay was much less pronounced, compared to PGK-Alexa 488 (Figure 4B and C). As we did not expect any rotational freedom of FlAsH with respect to helix A, this fast component reflected the relative movement of helix A with respect to the whole protein (segmental movement). The remaining fraction of the total decay is again related to whole-molecule rotation of CaM. In contrast, the anisotropy decay of calcium-activated CaM could be described by a single component, thus reflecting only the rather slow whole-molecule tumbling (similar to GFP, see Figure 4A, D). It is well known that calcium binding induces structural changes, with a more stretched and more rigid structure of Ca^{2+}–CaM (for example, "locking" the helix A movement) compare to apo-CaM.[21,29] The effect of this conformational change is clearly visible in our TRA data and is in qualitative agreement with data measured with the same kind of samples by a frequency domain approach.[18]

To summarize, our apo-CaM-FlAsH complex does not provide a fluorophore as rigidly crosslinked to the whole protein structure as in the case of GFP with the β-barrel, but it is clearly more rigidly attached to CaM than is the single-bonded maleimide functionalized dye with PGK. The practicability of FlAsH-labeled CaM to study the structural and dynamical properties of the protein was demonstrated in this comparative analysis, and it was next employed (in the apo form) for investigations of RNC complexes.

Fluorescence anisotropy decay of RNC constructs

For studying RNC complexes with nascent CaM chains of different lengths, cell-free protein synthesis was used. The properties of FlAsH-labeled purified RNC complexes (see the Experimental Section) were measured in the same way as for full-length CaM synthesized in vivo. We also measured the nascent CaM chains after release from the ribosome (induced by adding puromycin to the RNC complexes). Anisotropy decays were calculated and fitted with models as described above (Figure 5 and Table 2). Because of the rather small amounts of in vitro synthesized CaM chains, the statistics were not as good as those in the previous section. However, comparison of the data between those for full-length apo-CaM (Figure 4C) and for released full-length CaM chain (Figure 5A) demonstrates reasonable agreement of the obtained fit parameters (Tables 1 and 2). Both samples were best fitted with two components: a fast component (segmental motions) and a significantly slower component that describes whole-molecule tumbling. As the in vitro synthesized CaM chains included the linker and the SecM-arrest sequences (together ~4.7 kDa) the total molecular mass of the full-length construct here was 21.7 kDa (17.8 kDa for wild-type CaM). As a consequence, we observed a larger correlation time (θ_M) for the full-length released CaM chain (~11.57 ns; other apo-CaM-FlAsH construct ~6.59 ns). In accordance with Equation (1), for the released constructs we observed decreasing θ_M for whole-molecule

Table 2. Fitting parameter obtained from data in Figure 5.[a]

Sample	r_0	θ_1 [ns]	A_1	θ_M [ns]
full-length, released	0.245 [0.237–0.254]	0.91 [0.68–1.21]	0.7 [0.66–0.73]	11.57 [10.5–12.9]
full-length, tethered	0.234 [0.228–0.241]	1.82 [0.85–2.28]	0.86 [0.78–0.91]	24.6 [20.6–32.6]
half-length, released	0.24 [0.23–0.25]	1.17 [0.89–1.51]	0.56 [0.53–0.59]	5.12 [4.5–5.9]
half-length, tethered	0.26 [0.24–0.27]	0.3 [0.1–0.4]	0.71 [0.63–0.79]	16.6 [14.6–20.4]
EF-hand, released	0.26 [0.25–0.28]	0.51 [0.36–0.67]	0.29 [0.16–0.44]	2.1 [1.5–3.5]
EF-hand, tethered	0.14 [0.13–0.14]	–	–	14.0 [12.5–15.8]

[a] The fitting models are detailed in the Experimental Section. [b] The confidence interval is given in brackets, see the Experimental Section.

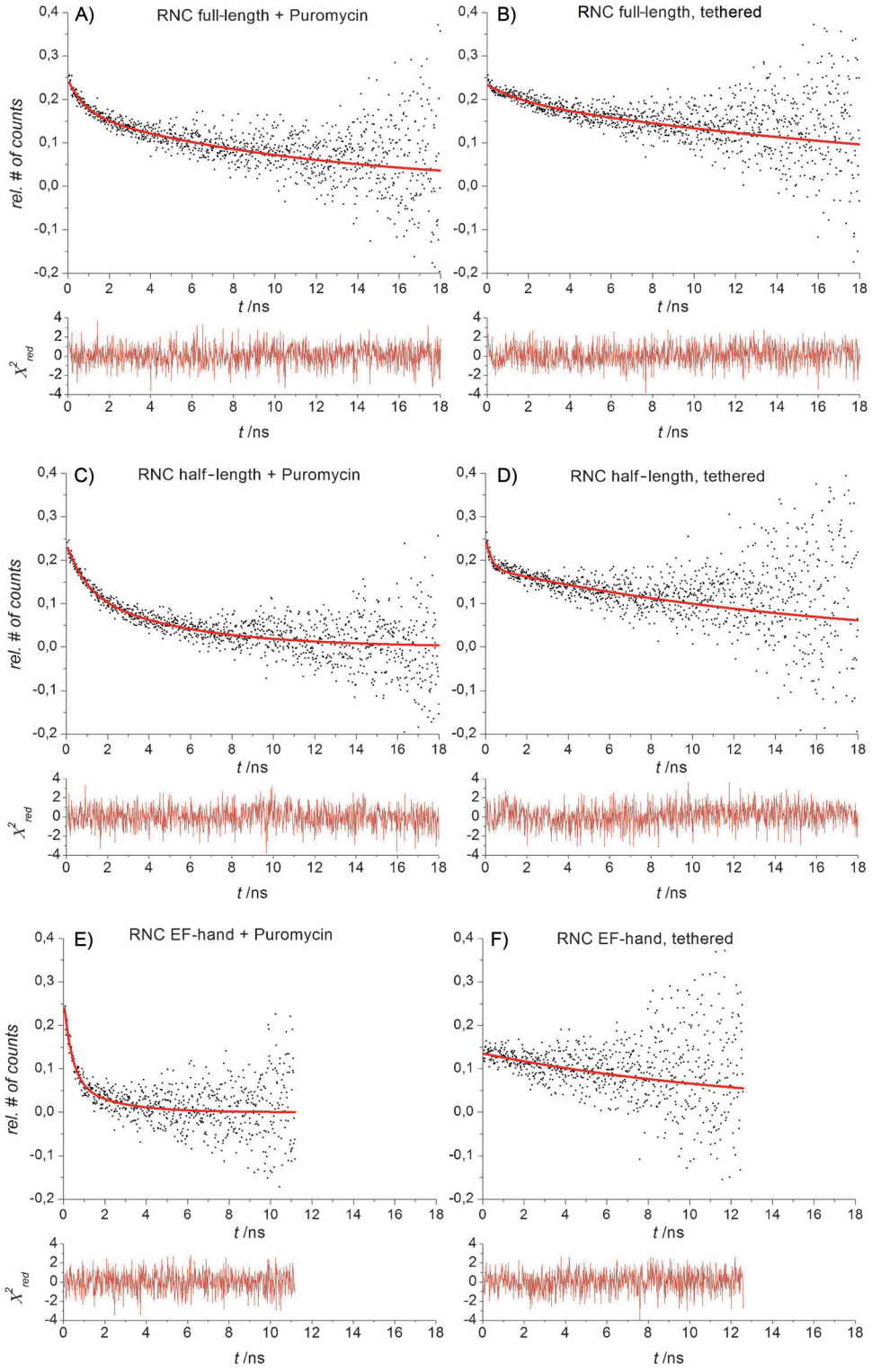

Figure 5. Time resolved anisotropy decays for CaM constructs: A) full-length released, B) full-length ribosome-tethered, C) half-length released, D) half-length ribosome-tethered, E) first EF-hand released, and F) first EF-hand ribosome-tethered.

tumbling with decreasing mass (other CaM-FlAsH constructs: CaM half-length 13.2 kDa; EF-hand 8.9 kDa). The fast segment motions of released constructs showed slight reduction in correlation times with decreasing size of construct. The corresponding A values show a clear decrease with decreasing construct length, thus indicating increased mobility of helix A. As the surrounding structural elements of helix A "lock" helix A orientation, we would expect a more flexible helix A when these elements are absent, as is definitely the case for the EF hand. However, a definitive conclusion about theses fast segmental motions is difficult, because the correlation times were at the limits of our resolution, and they became more biased with respect to the decreasing correlation times of the whole molecule rotation. In the case of ribosome-tethered CaM–FlAsH constructs the most reasonable model to describe the data would be one that assumes two restricted motions ("wobbling in a cone"), the internal segmental motion (θ_1, A_1) and, because of tethering, restricted motion of the whole CaM nascent chain construct (θ_2, A_2, see Equation (3)). In this model of restricted motion, the A values characterize the rotational freedom of the motion and are parameterized by the respective semicone angles[26] (for details see the Experimental Section). We performed fits by this approach and obtained A_2 values (the slower motions) below 0.1 (related to semicone angles $>65^\circ$; full rotational mobility is characterized by 90°). We applied the same approach with the data for released constructs and obtained similar results. In order to achieve a good comparability between the data for tethered and released constructs, we fitted all data with the simpler model, by employing one restricted motion and free whole-molecule tumbling (Table 2). The most striking difference between the released and tethered constructs was the significantly lower whole-molecule tumbling correlation time for the tethered constructs. Similarly to the released constructs, the tumbling correlation times for tethered constructs decrease with the mass of the

tumbling unit. For tethered and released constructs, the respective sizes of the CaM-constructs were the same. Hence the observed differences were caused most probably by the interaction of the nascent chains with the ribosome surface. As a consequence of tethering to the ribosome, more frequent collisions between the constructs and the ribosome increase an "apparent microviscosity", which results in larger correlation times [Eq. (1)]. Because of the poor statistics, the fast segment motions of the tethered constructs were not well resolved. Although for the full-length and half-length constructs small fast-decay components are visible (Figure 5B, D), this component is missing for the EF-hand (see Figure 5F), most probably attributable to scattering effects in deficient sample and background measurements. Therefore we were unable to process on fast timescales (<1 ns), and we obtain an r_0 value that is too small ($r_0 = 0.14$).

As FlAsH is rigidly bound to helix A in calmodulin (and in CaM constructs), the obtained data allowed us to monitor nanosecond reorientations of this helix under different environmental conditions. The fact that we were able to label the different constructs indicates that the required tetracysteine motif was formed, and that helix A (at least) was folded for all investigated constructs. Furthermore, the reasonable description of the observed correlation times for whole-molecule tumbling with Equation (1) and the obtained CD data indicate that a larger fraction of the nascent chain was folded (more than just helix A), particularly for the longer constructs. A comparative analysis between full-length apo-CaM and calcium activated CaM demonstrated that calcium binding induces much stronger binding of helix A to the rest of the protein, consistent with a previous report.[18] With the helix A acting as a "mobility probe" in the CaM constructs, we were (in principle) able to measure internal nascent chain dynamics (relative movements of the helix A with respect to the whole construct) as well as whole-molecule tumbling (helix movements when rigidly connected to the whole construct). The advantage here was that we did not suffer from pronounced fast decays (20–50% total decay amplitude) as is caused by dye rotations when conventional labeling techniques are employed (Figure 4B and other studies[11]). However, if the typical correlation times of internal movements (from one to a few nanoseconds) and those of whole-molecule rotations (from one to a few tens of nanoseconds) come close to each other, a clear distinction in no longer possible, particularly for small nascent chain constructs. In a study using a rather similar approach, Ellis and coworkers studied RNC complexes of apo-myoglobin with constructs of different length.[11] As they did not use constructs with C-terminal linker sequences spanning the ribosomal tunnel, they observed typical nascent chain dynamics (with correlation times of a few nanoseconds) only for constructs longer than 35 amino acids. Similarly to our results, theirs showed evidence that these ribosome-tethered nascent chains are compact and exhibit at least partial folding. The effect of slower apparent rotational chain motion for constructs tethered to the ribosome (compared to released constructs) was not observed in the study on apo-myoglobin. However, NMR studies[10,30] and force measurements[13] on RNC complexes have reported evidence of specific and transient interactions between the nascent chains and the ribosome surface. This is in line with our observation of reduced rotational tumbling motions; this might be caused by frequent collisions with the ribosome. Kaiser and co-workers argued that a specific nascent chain–ribosome surface interaction prevents misfolding and keeps the polypeptide chain in folding-competent conformation.[13] Thus the ribosome itself would act as a molecular chaperone for nascent polypeptide chains. Furthermore, there is strong evidence that the nascent chain interaction takes place directly with the ribosome surface and is not mediated by cotranslational chaperones (e.g., Trigger factor, DnaK), because ours and the force-based study employed the PURE in vitro protein synthesis system, which does not contain chaperones.

Conclusions

This study demonstrated that a biarsenical dye attached to a tetracysteine motif located in a helix of a protein is well suited to examining CaM fragments of different sizes. Without interference from convoluted probe-dye motions, a time window of one nanosecond up to a few tens of nanoseconds was achievable. Our approach can be used to characterize not only whole-molecule tumbling motions but also local segment motions. In an application to calmodulin fragments of different lengths we obtained insights about the folding of nascent chains. The in vitro synthesized polypeptide chains adopt partially folded structures and exhibit pronounced interactions with the ribosome surface in cases were the nascent chains remain tethered (through a linker sequence) to the ribosome. A major limitation of our approach is that short nascent polypeptide chains exhibit rather small correlation times for whole-molecule tumbling; this interferes with the corresponding correlation times of segment motions. Therefore, a possible field of future investigation would be to study proteins with large domains—many secondary structure elements that are synthesized sequentially and might alter the dynamical properties of our "mobility probe" during chain elongation and cotranslational folding. However, good statistics are always crucial to obtain meaningful characterization of the state of folding. The ultimate goal in studying cotranslational folding is real-time measurements during chain elongation.[30,31] This could be a development of the approach presented here (we studied "snap shots" in time by looking at a set of particular chain lengths). Although the use of FlAsH–helix constructs can in principle deliver time-resolved information, the statistic would be a limiting factor. This is not only a consequence of the relatively short observation times (if we aim for reasonable time resolution), but also because an ensemble of ribosomes will not provide synchronous chain elongation. Thus, single-molecule studies are required, although this would still cause problems with statistics. Although single-molecule studies with surface-immobilized CaM-FlAsH samples have been performed by Lu and coworkers,[22] real-time observation of the folding process with FlAsH (over at least a few tens of seconds for the whole synthesis) is presumably beyond the capabilities of this approach.

Experimental Section

PCRs and cloning: Based on the known sequence of the bovine CaM gene (UniProtKB: P62157), oligonucleotides with suitable cloning sites at their 5′-ends were used for the amplification and introduction of the mutation (E7C, E8C, A11C, E12C) into the genes by PCR from the wild-type CaM gene as the template (a kind gift from Prof. A. Baumann, Research Center Jülich, Germany). The forward primer contained an upstream NdeI restriction site and the mutated amino acid sequence; the reverse primer contained a downstream XhoI site. The mutated sequences of the amplified genes were cloned into a pRSET vector (Invitrogen) between the NdeI and XhoI restriction sites. The resulting proteins were fused to a linker rich in Ser and Gly followed by the SecM arrest sequence (FxxxxWIxxxxGIRAGP) taken from the secretion monitoring protein SecM, and were also cloned into the pRSET vector between the XhoI and HindIII sites.[32]

Gene sequences were verified by DNA sequencing. The same mutated genes were also cloned into a pET27b vector (His_6 tag fusions) for overexpression in *E. coli* and purification by affinity chromatography.

Purification of mutated CaM: The protein was purified according to the method of Zahn et al.[33] with some modifications. Cells were grown in selective DYT medium (100 mL, 16 g L^{-1} Bacto Tryptone, 10 g L^{-1} Bacto Yeast Extract, 5 g L^{-1} NaCl, 200 μg mL^{-1} ampicillin). CaM was overexpressed for 45 min after induction with isopropyl-β-D-thiogalactopyranoside (IPTG, 1 mM), when the culture had grown to $OD_{600}=0.5$. Cells were centrifuged (6000 *g*, 20 min, 4 °C), and the pellet was placed in lysis buffer (4-morpholinepropanesulfonic acid; MOPS (10 mM, pH 7.4), NaCl (500 mM), Gnd·HCl (6 M), tris-(2-carboxyethyl)phosphine hydrochloride (TCEP; 1 mM)). Cells were lysed by sonication, the lysate was centrifuged, and the supernatant was mixed with Ni-NTA beads for 3 h at 4 °C. The beads were washed with lysis buffer, and the concentration of Gnd·HCl was decreased by sequential washing steps with buffers containing Gnd·HCl (5, 4, 3, 2, and 1 M). Another washing with buffer without Gnd·HCl followed. The beads were washed three times with washing buffer (10 mM MOPS, 500 mM NaCl, 5 mM imidazole, 1 mM TCEP, pH 7.4). Three elution steps at room temperature with elution buffer (10 mM MOPS, 500 mM NaCl, 250 mM imidazole, 1 mM TCEP, pH 7.4) followed. Imidazole was removed by size-exclusion chromatography (Sephadex G-25).

Labeling with FlAsH: To label mutated CaM full-length with FlAsH, protein was dissolved in labeling buffer (10 mM MOPS, 500 mM NaCl, 1 mM TCEP, pH 7.4) to a final concentration of 20 μM in a low-adhesion Eppendorf tube, the mixture was degassed for 30 min under 250 mbar vacuum and left at room temperature for 2.5 h, so that disulfide bonds were reduced. FlAsH was added to a final concentration of 4 μM in the presence of nitrogen gas. The concentration ratio between protein and FlAsH was 5:1. This was necessary so that most of the dye molecules (90–100%) were attached to the tetra-Cys motif. The labeling reaction took place at 37 °C in complete darkness for 3 h. Finally, the sample was stored at 4 °C, again in complete darkness, for two days. Any excess FlAsH was removed by size-exclusion chromatography (Sephadex G-25).

Circular dichroism spectroscopy: A J-810 spectropolarimeter (JASCO) was used to measure CD spectra in the far-UV region (200–280 nm). The spectra were recorded at 20 °C in a 0.1 cm cell at protein concentration of 0.2 mg mL^{-1}; data were averaged from two scans (scan rate 50 nm min^{-1}). A buffer spectrum was also measured, and subsequently subtracted from raw sample data.

Preparation and purification of labeled RNCs: The in vitro transcription-translation reactions were performed with the PURExpress in Vitro Protein Synthesis kit (NEB, Ipswich, MA)[34] by following the manufacturer's instructions. An oligonucleotide having the antisense sequence of tmRNA (5′-TTAAG CTGCT AAAGC GTAGT TTTCG TCGTT TGCGA CTA-3′) was also added to a final concentration of 5 nM. The above labeling protocol was followed but with the difference that Tico buffer (HEPES (20 mM, pH 7.6), $(CH_3COO)_2Mg$ (6 mM), CH_3COONH_4 (30 mM)) was used. Excess dye was removed by size-exclusion chromatography (Sephadex G-75). Where needed, the nascent CaM chains were released from the ribosome by adding puromycin (1.3 mM, Sigma–Aldrich) for 10 min at 37 °C. The fractions with labeled RNCs were selected by performing steady-state fluorescence anisotropy measurements. The steady-state anisotropy, r_{ss}, was calculated from $r_{ss}=(I_{\parallel}-GI_{\perp})/(I_{\parallel}+2GI_{\perp})$, where $I_{\parallel}$ and $I_{\perp}$ are the intensities of the parallel and perpendicular components with respect to the polarization of the excitation beam. A QM-7 spectrofluorometer (Photon Technology International, Birmingham, NJ) was used. Each time steady-state anisotropy was measured (20 °C), excitation and emission polarizers (2 mm slit width) were used. The fluorescence intensities of polarization components were also corrected for transmission efficiencies of the monochromator (G-factor, *G*).

Time-resolved fluorescence anisotropy measurements and data analysis: Time-resolved fluorescence anisotropy measurements with diffusing molecules were performed with a MicroTime 200 confocal microscope (PicoQuant, Berlin, Germany). The fluorophores were excited with linear polarized light from a 470 nm pulsed laser diode (20 MHz repetition rate, ~30 μW average excitation power). The samples (typically 300 μL) were placed on cleaned cover-glass slides treated with Sigmacote (Sigma–Aldrich). The fluorescence collected by an UplanSApo objective (60×/1.2w; Olympus, Hamburg, Germany) passed through a 50 μm pinhole and thereafter a mounted Glan–Thompson calcite polarizer attached to a precision cage rotation mount (Thorlabs, Newton, NJ). By adjusting the polarizer to 0 and 90° (with respect to polarization of excitation light), the parallel and perpendicular, respectively, polarized fluorescence emission components were selected. After passing through emission filters (FF01-520/35, lot: 112217-112224, AHF, Tübingen, Germany), the fluorescence was detected by SPCM-AQ14 avalanche photodiodes (PerkinElmer) and the arrival time of each detected photon was recorded by a PicoHarp 300 time-correlated single photon counting (TCSPC) card (PicoQuant). Data were analyzed and displayed by using custom-written Matlab routines (Figure 6A). All measurements were performed at 20 °C with protein (a few nanomolar) and Tween 20 (0.001%, *w/v*) in buffer (10 mM MOPS, 50 mM NaCl, pH 7.4). Time-resolved anisotropy decays were calculated according to Equation (2). See also Figure 6B.

$$r(t)=\frac{I(t)_{\parallel}-G\cdot I(t)_{\perp}}{I(t)_{\parallel}+2G\cdot I(t)_{\perp}} \qquad (2)$$

To eliminate background noise, the background signals for parallel and perpendicularly polarized emission from the buffer solution were measured and subsequently subtracted from the data. The dependency of the detection efficiency on polarization was taken into account through the "*G*-factor" (*G*). *G* was determined by measuring a nanomolar solution of Alexa 488 in water (this has a spectrum similar to FlAsH; additionally, Alexa 488 is known to have a sub-nanosecond rotational correlation time and does not show any residual anisotropy). Therefore, the *G*-factor was adjusted to the value the time-resolved anisotropy curve of Alexa 488 de-

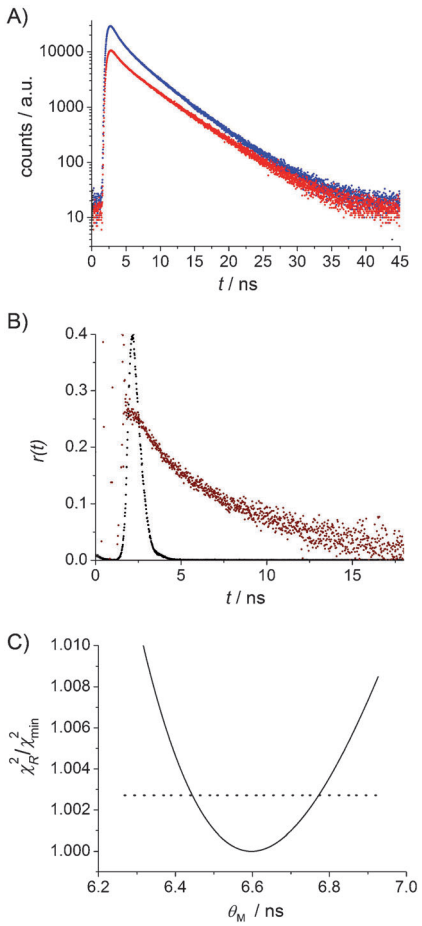

Figure 6. Example of measured data, calculated functions, and statistical analysis of fitting results are shown for data obtained from apo-CaM labeled with FlAsH (see Figure 3C and Table 1). A) Measured $I_{\parallel}(t)$ (blue) and $I_{\perp}(t)$ (red). B) The corresponding $r(t)$ (red) data calculated from $I_{\parallel}(t)$, $I_{\perp}(t)$, and the G-factor [Eq. (2)] as well as the corresponding instrument response function (IRF; black) are shown. C) Result of supported-plane analysis with the respective confidence interval (6.4–6.77 ns), limited by the intersections of both lines, is shown for the fitting parameter θ_M. · · · · : F_χ, ——: χ^2_R/χ^2_{min}.

cayed to zero for times well above 4 ns. To fix the starting point of the $r(t)$ curves, the instrument response function (IRF) was recorded before every measurement by using Ludox TMA colloidal silica scattering medium (Sigma–Aldrich; 1:1000 in water; Figure 6B). The starting point of $r(t)$ was then set to lie under the peak of the IRF profile. As the parallel and perpendicular polarized fluorescence emission components were detected with the same avalanche photodiode, the influence of the IRF was assumed to be relatively small and was not taken into account by reconvolution. For data interpretation, $r(t)$ curves were fitted with rotational diffusion models by using a weighted nonlinear least-squares minimization function implemented in Matlab. All tested models (e.g., free spherical rotator, restricted motion described by the "wobbling-in-a-cone" model) were simplified cases of the rather complex "cone-in-a-cone" model[26] of Equation (3):

$$r(t) = r_0 \cdot \left[(1-A_1)e^{-t/\theta_1} + A_1\right] \cdot \left[(1-A_2)e^{-t/\theta_2} + A_2\right] \cdot e^{-t/\theta_M} \qquad (3)$$

here r_0 represents the fundamental anisotropy, $\theta_{,2}$ and $\theta_{,2}$ are the correlation times of the restricted motions, and θ_M is the correlation time of whole-molecule tumbling. The related amplitude factors for the restricted motions $A_{1,2}$ are related by the equation for the respective semi-cone angles $\phi_{1,2}$:

$$A_{1,2} = \left[\frac{1}{2}\left(1+\cos\phi_{1,2}\right)\cos\phi_{1,2}\right]^2 \qquad (4)$$

Reasonable fits showed residuals fluctuating randomly around zero without any systematic deviations. In addition, reduced χ^2 values should show values close to unity with the lowest possible number of free parameters.

To estimate the confidence intervals of the determined parameters, a support-plane analysis was implemented in Matlab and applied to the fitting results (Figure 6C). The procedure is to fix a parameter of interest to a value different from the value yielding the minimal χ^2. Subsequently, the fit is rerun so that the other parameters have to adjust, now with a new minimal χ^2. Further shifts and refit procedures are repeated until the new minimal χ^2 is not acceptable anymore as judged by F-statistics.[27] As discussed in detail in ref. [27], the obtained widths of the confidence intervals are systematically too small in this analysis. A more realistic interval width is obtained by reducing the degrees of freedom (200 instead of ~1000 independent data points) which results in larger $F\chi$ values (i.e., raising the dotted line in Figure 6C). This adaptation would typically lead to three- to fourfold larger confidence intervals for the obtained fitting parameters (e.g., θ_M with 6.18–7.23 instead of 6.4–6.77, in Figure 6C).

Acknowledgements

P.L. acknowledges the International Helmholtz Research School on Biophysics and Soft Matter (Biosoft) for support. We thank Prof. Dr. Arnd Baumann (ICS-4: Cellular Biophysics, Forschungszentrum Jülich GmbH) for providing us with the gene of wild-type calmodulin. Henning Höfig is acknowledged for help with displaying FlAsH docked to calmodulin and Ramona Justinger and Ilona Ritter for helping us with the sequencing of DNA constructs. Furthermore, we would like to thank Sena Ledesch for measurements of the PGK-Alexa 488 sample.

Keywords: biosynthesis · cotranslational protein folding · fluorescence anisotropy decay · nascent polypeptide chains · proteins

[1] W. Kudlicki, J. Chirgwin, G. Kramer, B. Hardesty, *Biochemistry* **1995**, *34*, 14284–14287.
[2] V. A. Kolb, E. V. Makeyev, A. S. Spirin, *EMBO J.* **1994**, *13*, 3631–3637.
[3] A. N. Fedorov, T. O. Baldwin, *J. Biol. Chem.* **1997**, *272*, 32715–32718.
[4] G. Zhang, Z. Ignatova, *Curr. Opin. Struct. Biol.* **2011**, *21*, 25–31.
[5] C. B. Anfinsen, *Science* **1973**, *181*, 223–230.
[6] A. H. Elcock, *PLoS Comput. Biol.* **2006**, *2*, e98.
[7] J. Frydman, H. Erdjument-Bromage, P. Tempst, F. U. Hartl, *Nat. Struct. Biol.* **1999**, *6*, 697–705.
[8] P. L. Clark, J. King, *J. Biol. Chem.* **2001**, *276*, 25411–25420.
[9] C. A. Woolhead, P. J. McCormick, A. E. Johnson, *Cell* **2004**, *116*, 725–736.
[10] S.-T. Hsu, P. Fucini, L. D. Cabrita, H. Launay, C. M. Dobson, J. Christodoulou, *Proc. Natl. Acad. Sci. USA* **2007**, *104*, 16516–16521.
[11] J. P. Ellis, C. K. Bakke, R. N. Kirchdoerfer, L. M. Jungbauer, S. Cavagnero, *ACS Chem. Biol.* **2008**, *3*, 555–566.
[12] A. Khushoo, Z. Yang, A. E. Johnson, W. R. Skach, *Mol. Cell* **2011**, *41*, 682–692.
[13] C. M. Kaiser, D. H. Goldman, J. D. Chodera, I. Tinoco Jr., C. Bustamante, *Science* **2011**, *334*, 1723–1727.

[14] D. Kajihara, R. Abe, I. Iijima, C. Komiyama, M. Sisido, T. Hohsaka, *Nat. Methods* **2006**, *3*, 923 – 929.
[15] I. Saraogi, D. Zhang, S. Chandrasekaran, S.-o. Shan, *J. Am. Chem. Soc.* **2011**, *133*, 14936 – 14939.
[16] S. Milles, S. Tyagi, N. Banterle, C. Koehler, V. VanDelinder, T. Plass, A. P. Neal, E. A. Lemke, *J. Am. Chem. Soc.* **2012**, *134*, 5187 – 5195.
[17] S. R. Adams, R. E. Campbell, L. A. Gross, B. R. Martin, G. K. Walkup, Y. Yao, J. Llopis, R. Y. Tsien, *J. Am. Chem. Soc.* **2002**, *124*, 6063 – 6076.
[18] B. Chen, M. U. Mayer, L. M. Markillie, D. L. Stenoien, T. C. Squier, *Biochemistry* **2005**, *44*, 905 – 914.
[19] R. Liu, D. Hu, X. Tan, H. P. Lu, *J. Am. Chem. Soc.* **2006**, *128*, 10034 – 10042.
[20] P. James, T. Vorherr, E. Carafoli, *Trends Biochem. Sci.* **1995**, *20*, 38 – 42.
[21] D. Chin, A. R. Means, *Trends Cell Biol.* **2000**, *10*, 322 – 328.
[22] X. Tan, D. Hu, T. C. Squier, H. P. Lu, *Appl. Phys. Lett.* **2004**, *85*, 2420 – 2422.
[23] S. R. Adams, R. Y. Tsien, *Nat. Protoc.* **2008**, *3*, 1527 – 1534.
[24] R. Y. Tsien, *Annu. Rev. Biochem.* **1998**, *67*, 509 – 544.
[25] T. Rosenkranz, R. Schlesinger, M. Gabba, J. Fitter, *ChemPhysChem* **2011**, *12*, 704 – 710.
[26] G. F. Schröder, U. Alexiev, H. Grubmüller, *Biophys. J.* **2005**, *89*, 3757 – 3770.
[27] J. R. Lakowicz, *Principles of Fluorescence Spectroscopy*, Kluwer Academic/Plenum, New York, **1999**.
[28] J. García de la Torre, *Biophys. Chem.* **2001**, *93*, 159 – 170.
[29] J. J. Chou, S. Li, C. B. Klee, A. Bax, *Nat. Struct. Biol.* **2001**, *8*, 990 – 997.
[30] L. D. Cabrita, C. M. Dobson, J. Christodoulou, *Curr. Opin. Struct. Biol.* **2010**, *20*, 33 – 45.
[31] A. Katranidis, D. Atta, R. Schlesinger, K. H. Nierhaus, T. Choli-Papadopoulou, I. Gregor, M. Gerrits, G. Büldt, J. Fitter, *Angew. Chem. Int. Ed.* **2009**, *48*, 1758 – 1761; *Angew. Chem.* **2009**, *121*, 1790 – 1793.
[32] A. Rutkowska, M. Beerbaum, N. Rajagopalan, J. Fiaux, P. Schmieder, G. Kramer, H. Oschkinat, B. Bukau, *FEBS Lett.* **2009**, *583*, 2407 – 2413.
[33] R. Zahn, C. vonSchroetter, K. Wüthrich, *FEBS Lett.* **1997**, *417*, 400 – 404.
[34] Y. Shimizu, A. Inoue, Y. Tomari, T. Suzuki, T. Yokogawa, K. Nishikawa, T. Ueda, *Nat. Biotechnol.* **2001**, *19*, 751 – 755.

Received: January 6, 2014
Published online on March 18, 2014